

## Photocatalytic Degradation of Synthetic Dyes using Iron (III) Oxide Nanoparticles (Fe<sub>2</sub>O<sub>3</sub>-Np) Synthesized using *Rhizophora mucronata* Lam.

Nathan Vinod Kumar<sup>1</sup>, Parvathi Ammini<sup>1\*</sup>, Jasna Vijayan<sup>1</sup>

<sup>1</sup>National Institute of Oceanography-CSIR, Regional Centre,  
Dr. Salim Ali Road, Cochin 682018, Kerala, India

\*parvathi@nio.org

### Abstract:

Biosynthesis of nanoparticles through plant extracts are gaining attention due to the toxic free synthesis process. The environmental engineering applications of many metal oxide nanoparticles have been reported. Recently, metal nanoparticles and metal oxide nanoparticles are used as nano-adsorbents, nano-catalysts, nano-filtration, and nano-biocides for remediation of water and wastewater pollutants. In this study, iron oxide nanoparticles (Fe<sub>2</sub>O<sub>3</sub>-Nps) were synthesized using a simple biosynthetic method using a leaf extract of a mangrove plant *Rhizophora mucronata* through reduction of 0.01 M ferric chloride. Fe<sub>2</sub>O<sub>3</sub>-Np synthesis was revealed by a greenish colour formation with a surface plasmon band observed close to 368 nm. The stable Fe<sub>2</sub>O<sub>3</sub>-Np possessed excitation and emission wavelength of 368.0 and 370.5 nm respectively. The FTIR spectral analysis revealed the changes in functional groups during formation of Fe<sub>2</sub>O<sub>3</sub>-Np. Agglomerations of nanoparticles were observed during Scanning electron microscopic (SEM) analysis and Energy-dispersive X-ray spectroscopic analysis (EDAX) analysis confirmed the ferric oxide nature. The average particle size of Fe<sub>2</sub>O<sub>3</sub>-Np based on dynamic light scattering (DLS) was about 65 nm. Based on transmission electron microscopic (TEM) analysis, particles were spherical in shape and the crystalline size was confirmed by selected area electron diffraction (SAED) pattern analysis. The synthesized Fe<sub>2</sub>O<sub>3</sub>-Np exhibited a good photodegradation efficiency with a reduction of 83 and 95% of phenol red and crystal violet under irradiation of sunlight and florescent light respectively. This report is a facile synthesis method for Fe<sub>2</sub>O<sub>3</sub>-Np with high photodegradation efficiency.

## 1. Introduction

Nanotechnology is a tool of the recent decade to resolve many issues related to environment and health care. The nano-scale particles have numerous advantages and is widely explored for its new functionalities. The metal nanoparticles production is usually carried out using physical and chemical methods. An array of chemicals is required for the metal nanoparticles production, which are very reactive and toxic reducing agents. This brings about many deleterious effects during its application in health care and environmental engineering. In the meantime, many facile and reliable green technologies were adopted for the production of these nanoparticles. Among the green technologies, various organisms act as precursors to produce the stable and well functionalised nanoparticles, which includes bacteria, actinomycetes, fungi, yeast, viruses, plants, etc. [1, 2]. Plant mediated nanoparticle synthesis is more reliable in terms of its monodispersed nature, stability and fast synthesis compared to other precursors [3, 4]. Various part of plants can be used for the metal nanoparticle synthesis and the process is the simplest and most cost-effective [5].

The environmental engineering applications of many metal oxide nanoparticles, especially iron oxide nanoparticles have been reported. Recently, metal nanoparticles and metal oxide nanoparticles are used as nano-adsorbents, nano-catalysts, nano-filtration, and nano-biocides for remediation of water and wastewater pollutants. Among them, potential of iron nanoparticles was found suitable for environmental remediation. The nanoscale zero-valent iron

has a large surface area to volume ratio, which enhances their reactivity especially in the environmental applications [6].

In the present work, we used *Rhizophora mucronata* a common mangrove plant for the synthesis of iron (III) oxide nanoparticles. The mangrove plants such as *R. mucronata* and *R. apiculata* were used for metal Np synthesis through bio-reduction method [7], which were proved to have antimicrobial [8] and anti-larvicidal activity [9]. However, there are no reports pertaining to the iron oxide nanoparticle synthesis using *R. mucronata* and hence this form the first report on the iron oxide nanoparticle synthesis to the best of our knowledge.

The dye decolourisation using biological system is a complex process requiring a suitable enzyme system in bioremediation of such effluents. Such dye rich effluents can be treated through metal oxide nanoparticle by the photocatalytic degradation process. Photocatalytic reactions are induced by the illumination of nano-sized semiconductors such as TiO<sub>2</sub>, ZnO, ZnS, WO<sub>3</sub> and Fe<sub>2</sub>O<sub>3</sub> in a suspension and they are most promising for the wastewater treatment [10] because of their high stability, low costs, high efficiency and no toxicity [11]. Among various semiconductor used in photo catalysts, iron oxide nanomaterials exhibit promising photocatalytic activities [12, 13, 14]. But, “combinational” nanoparticle

systems were used previously for the dye photocatalytic degradation activity. However, in the present study, we focused on the application of iron oxide nanoparticles ( $\text{Fe}_2\text{O}_3\text{-Np}$ ) alone in the photocatalytic degradation activity of some selected synthetic dyes.

## 2. Materials and Methods

### 2.1 Extract preparation

*Rhizophora mucronata* Lam. leaves were collected from Mangalavanam mangrove ecosystem, Kerala, India. The leaves were washed well to remove excess salt and dust particles. A 5 g of leaves was weighed and chopped into small pieces and an extract was made by boiling in milipore water for 5 min. The leaves were removed by filtration and the filtrate was used for nanoparticle synthesis.

### 2.2 Synthesis of Fe-nanoparticles

$\text{FeCl}_3$  (Sigma Aldrich) solution of two different concentrations (0.1 M and 0.01 mM) was made using milipore grade water. This solution was added to an equal amount of plant extract (1:1 v/v) while mixing. The colour change was observed while adding the solutions which confirmed the  $\text{Fe}_2\text{O}_3\text{-Np}$  synthesis.

### 2.3 Characterization of Fe-nanoparticles

Based on the colour change, the nanoparticle synthesis was initially screened and the sample was subjected to scanning in the range of 200-800 nm using UV-Vis spectrophotometer (Spectronic-200, Thermo Scientific, USA). The absorbance maximum of the nanoparticle solution was noted. The nanoparticle sample and plant extract was subjected to FT-IR analysis (FT-IR Prestige 21 Shimadzu) in the range of 4000-400  $\text{cm}^{-1}$  for understanding the functional groups involved. Particle size of the synthesized nanoparticle was determined by dynamic light scattering (DLS) (Malvern Instruments Ltd.). The sample was further centrifuged and dried overnight for Scanning Electron Microscopy (SEM) (JEOL Model JSM - 6390LV), Energy-dispersive X-ray spectroscopic analysis (EDAX), and X-ray Diffraction (XRD) analysis using X-ray Diffractometer (Bruker AXS D8 Advance). Excitation and emission properties of the  $\text{Fe}_2\text{O}_3\text{-Np}$  synthesized were analysed by spectrofluorometric analysis using Spectrofluorometer (SL-174, Elico, India). Further characterization was carried out using high resolution Transmission electron microscopy (HR-TEM) and selected area electron diffraction (SAED) pattern.

### 2.4 Photocatalytic degradation of synthetic dyes using Fe-Np

The photocatalytic degradation activities of synthesized  $\text{Fe}_2\text{O}_3\text{-Np}$  samples were analyzed using various concentrations of synthetic dyes under different light sources. For the experiment, four synthetic dyes namely phenol red (PR), rhodamine B (RB), acridine orange (AO) and crystal violet (CV) were used. Three different conditions were applied to the photo-catalysis reaction by illumination through fluorescent light, sunlight and UV light. The solution was stirred well before the illumination. The vials containing dyes +

Fe<sub>2</sub>O<sub>3</sub>-Np were incubated under illuminated conditions for 30 min and absorbance was measured at 554, 525, 590 and 570 nm for RB, AO, CV and PR respectively, using UV-visible spectrophotometer. The decolourisation efficiency was calculated using the formula:  $(A_0 - A_t)/A_0 \times 100$ , where A<sub>0</sub> is the absorbance before irradiation and A<sub>t</sub> is the absorbance at time t [15]. The absorbance contributed by nanoparticles was subtracted from test solution (kept as control) in the experiment.

### 3 Results and Discussion

#### 3.1 Spectroscopic analysis of iron oxide nanoparticles

The colour change of the extract from colourless to greenish-black was observed immediately after mixing, which indicated the formation of iron oxide nanoparticles. The time required for the bio-reduction of the metal ions varied from a few minutes as in *Euphorbia milli* to about 24 hrs as in lemon grass tea. When the *R. mucronata* leaf extract and FeCl<sub>3</sub> solution was mixed, a colour change was observed from yellowish brown to finally dark green, almost blackish green colour indicating the formation of Fe<sub>2</sub>O<sub>3</sub>-Np. In a previous work on Fe<sub>2</sub>O<sub>3</sub>-Np synthesis using neem leaves extract also, a similar change in colour was noticed [16]. During the excitation of surface plasmon resonance (SPR), there was a visible change in colour which was characterized by UV-VIS spectroscopy that could be due to the formation Fe<sub>2</sub>O<sub>3</sub>-Np [17]. Generally, the iron oxide nanoparticles have been prepared by strong hydrolysis of iron salts at elevated temperature [18]. The plant mediated iron (III) oxide nanoparticles (Fe<sub>2</sub>O<sub>3</sub>-Np) were prepared at room temperature in our study. Due to the high organic contents in the plant extracts, the mechanism study of iron oxide nanoparticles formation is bit difficult. However, the organic compound present in the plant extracts act as a reducing as well as capping or binding agent to form iron oxide nanoparticles [19].

UV-visible spectroscopy is most widely used technique to investigate the optical properties of the particles. UV-visible spectroscopy analysis was carried out in the range of 200-800 nm and the maximum absorbance was observed at 368 nm that may be due to the formation of iron (III) oxide nanoparticles due to the excitation of surface plasmon vibrations (Fig.1a). UV-VIS spectrum, known as the surface plasmon absorption band, of the individual nanoparticles is different from that of nanoparticles aggregate. The SPR of a nanoparticle aggregate is shifted to a longer wavelength as compared with SPR of the individual particles [20]. The shorter UV absorption wavelength confirmed that no aggregation of Nps occurred during the synthesis. Metallic iron nano particles synthesized in the present work exhibited a relatively identical UV-visible spectrum obtained from previous reports [21].

However, the UV visible spectrum of Fe<sub>3</sub>O<sub>4</sub>-Nps in the aqueous *Sargassum muticum* extract had two absorption peaks at wavelengths of 402 and 415 nm indicating the formation of ferrous oxide nanoparticles [22]. Similarly, nanoparticle synthesized using *Eucalyptus globulus* leaf extract mixture exhibited an absorption maximum ( $\lambda$  max) peak around 402 nm indicating the formation of low dimensional  $\beta$ -Fe<sub>2</sub>O<sub>3</sub>

[19]. UV-visible spectrum was observed for the extract with 0.1 M and 0.01 mM of FeCl<sub>3</sub> solution exhibited similar  $\lambda$  max. In the present study, the results depicted that 0.01 M was the optimum FeCl<sub>3</sub> concentration for the synthesis of Fe<sub>2</sub>O<sub>3</sub>-Np. Excitation and emission properties of the Fe<sub>2</sub>O<sub>3</sub>-Np synthesized were analysed by spectrofluorometric analysis (Fig 1b). The Fe<sub>2</sub>O<sub>3</sub>-Np exhibited an excitation at 368 nm and emission at 370.5 nm with a quantum yield (QY) of 1.0045. This result shows the possible application of the synthesized Fe<sub>2</sub>O<sub>3</sub>-Np in bio-imaging.

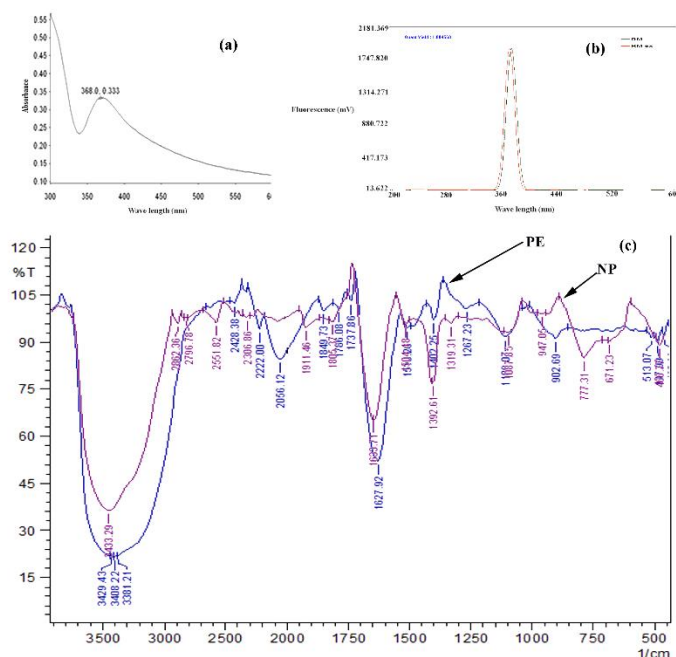


**Fig 1:** Characterization of Iron nanoparticle synthesized by *Rhizophora mucronata*- a) UV-Vis Spectrum b) Photoluminescence spectrum and c) FT-IR spectrum

### 3.2 FTIR analysis of synthesized iron oxide nanoparticles

The iron (III) oxide nanoparticles synthesized by *R. mucronata* was subjected to FTIR analysis and compared with the plant extract (before reaction). The FTIR spectrum of Fe<sub>2</sub>O<sub>3</sub>-Np (Fig 1c) represents the major absorption bands. The bands/peak assignments from the FTIR spectrum of Fe<sub>2</sub>O<sub>3</sub>-Np were: 3433.29- Br (OH) a characteristic N-H vibration region; 2862.36 - hydroxyl compounds; 2796.78- C-H stretch of aldehyde; 2551.82- -SH stretch; 2306.86-S=O Stretching; 1911.46 - N=C=S stretching; 1805.37- C=O stretching; 1633.71-C=C, alkene; 1504.48-C=C stretching – alkenes; 1392.61- C-H deformation due to alkynes; 1319.31 - NO<sub>2</sub> Nitro Compounds; 1087.85- C-O stretching due to secondary alcohols; 777.31 - C-H alkenes; 671.23- C-Br stretch of halogen groups and 466.77- metal oxide or metal chloride. The bands at 466.77 cm<sup>-1</sup> were due to the formation of metal oxides or metal chlorides [23, 24]. Bands at 3429.43, 3408.22 and 3381.21 cm<sup>-1</sup> were not visible in the FTIR spectrum of nanoparticle. Similarly, bands at 2056.12 and 902.69 cm<sup>-1</sup> were disappeared. Moreover, there was visible shift of peaks during the nanoparticle formation that might be due to oxido-reductive reactions. The results were comparable with

previous reports of Balamurugan et al., [19]. The presence of phenolic compounds and proteins might be responsible for the formation and stabilization of synthesized iron oxide nanoparticles [19].

### 3.3. XRD analysis of synthesized iron oxide nanoparticles

The average size, the crystalline nature of the particles and quality of compounds were determined by X-ray diffraction (XRD) spectrum with  $\text{CuK}\alpha$  radiation  $\lambda=1.504\text{\AA}$  over a wide range of Bragg angles using X-ray diffraction patterns (Fig. 2a). The XRD spectrum showed different diffraction peaks at  $12.02^\circ$ ,  $23.83^\circ$ ,  $31.92^\circ$  and  $45.81^\circ$  corresponding to the crystal planes of (220), (311), (422) and (440) of crystalline  $\text{Fe}_2\text{O}_3$ . The obtained data matched with the Joint Committee on Powder Diffraction Standards (JCPDS) File No. (4-755). Previously, major characteristic peaks for prepared crystalline metallic nanoparticles were obtained at  $2\theta$  values of 24.2, 33.1, 35.7, 40.9, 49.4, 54.1, 57.6, 62.6, and 64.0 degrees corresponding to (012), (104), (110), (113), (024), (116), (018), (214), and (300) respectively [19]. The average lattice size found for  $\text{Fe}_2\text{O}_3$ -Np ranged from 1.14 to 4.55 nm with a lattice strain of 0.0204 to 0.304. EDAX also supported the oxide nature of the nanoparticle (Fig 2 b).

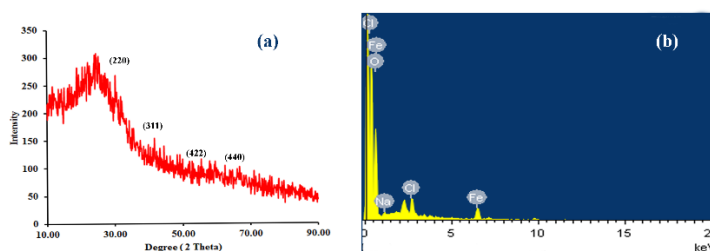


**Fig 2:** (a)XRD spectrum of  $\text{Fe}_2\text{O}_3$ -Np and (b) EDAX

### 3.4 SEM analysis of synthesized iron oxide nanoparticles

The dry powdered sample was analyzed for the structure and morphology of the synthesized  $\text{Fe}_2\text{O}_3$ -Np using SEM at different magnification levels (Fig 3a). SEM images revealed that the synthesized  $\text{Fe}_2\text{O}_3$ -Np were aggregated as irregular sphere shapes with rough surfaces. The morphology of the nanoparticles mostly appeared to be a porous and spongy. Based on the DSL method the average particle size was about 65 nm. However, agglomerations were observed similar to the previous report of Balamurugan et al., [19]. However, larger  $\text{Fe}_3\text{O}_4$ -Np with an average diameter of 116 nm was also reported [25]. Stability of the  $\text{Fe}_2\text{O}_3$ -Np was carried out after 3 months, and the peak position was stable.

### 3.5. TEM analysis

In the present work, the TEM images of the synthesized  $\text{Fe}_2\text{O}_3$ -Np showed spherical morphologies with 5.58 – 9.02 nm size (Fig 3 c and d). This was in agreement with the SAED results (6.04-8.3 nm) (Fig 3e).

$\alpha$ -Fe<sub>2</sub>O<sub>3</sub> nanoparticles synthesized by using green tea (*Camellia sinensis*) leaf extract resulted in spherical and highly porous particles with an average diameter of 60 nm based on the TEM images [26].

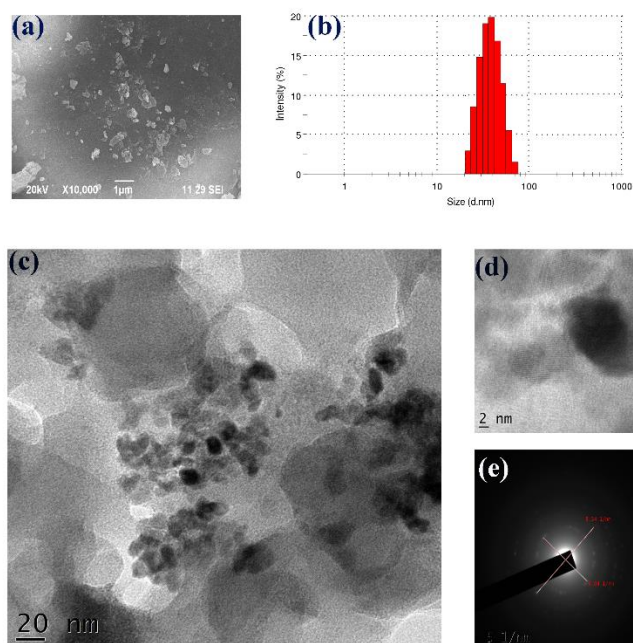


**Fig 3:** Morphological and size characterization of Fe<sub>2</sub>O<sub>3</sub>- Np synthesized by *Rhizophora mucronata* a) SEM image b) particle size distribution c) HR-TEM image d) magnified Fe<sub>2</sub>O<sub>3</sub>- Np and e) SAED

### 3.5 Photocatalytic degradation of synthetic dyes

The photocatalytic degradation of four dyes was carried out under three different illumination conditions. The Fe<sub>2</sub>O<sub>3</sub>-Np concentration when increased had enhanced the photocatalytic degradation of all dyes. Rhodamine B, phenol red and acridine orange exhibited maximum degradation at highest Fe<sub>2</sub>O<sub>3</sub>-Np concentration when incubated under sunlight (Fig 4). Whereas, in the case of crystal violet, maximum degradation was observed under fluorescent light followed by UV light source. Crystal violet showed minimal degradation under sunlight. The photo-oxidation of rhodamine B was carried out in the presence of H<sub>2</sub>O<sub>2</sub>/ Fe<sup>2+</sup> ion using UV light [27]. In a similar study, Alshehri et al., [28] observed that the Fe nanoparticles degraded more than 55% of congo red within a short period of 30 min under UV irradiation. However, a better degradation was observed in our study with a reduction of 83% and 95% of phenol red and crystal violet under irradiation of sunlight and florescent light respectively. At high concentrations, most of the dye molecules, after being adsorbed on the surface of Fe nanoparticles, may block the active reaction sites and might result in a decrease in the photodegradation efficiency [29]. In a previous study, they obtained maximum photodegradation efficiency with a concentration of 60  $\mu\text{g mL}^{-1}$  [28]. However, the concentration required in our study was very minimum as 50  $\mu\text{g mL}^{-1}$ .

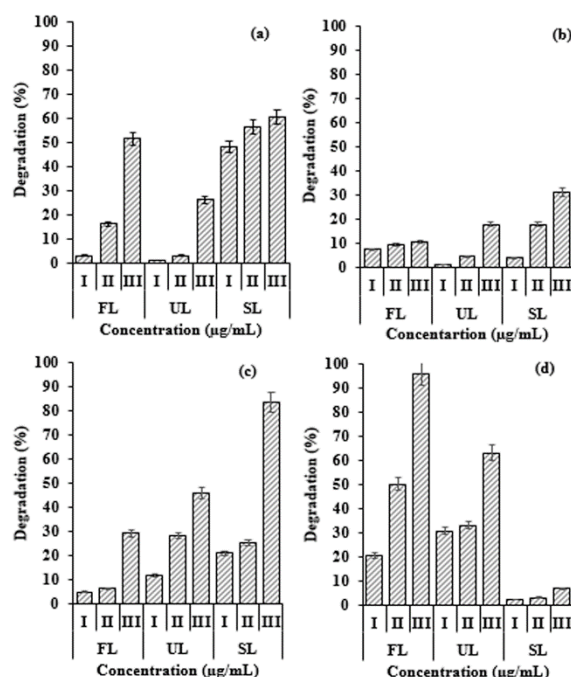


**Fig 4:** Photocatalytic degradation of synthetic dyes

a) rhodamine b) acridine orange c) phenol red and d) crystal violet [I-10; II- 25 and III-50  $\mu\text{g mL}^{-1}$ ; FL- fluorescent light; UL- UV light and SL- sunlight]

#### 4 Conclusion

Biogenic synthesis of iron (III) oxide nanoparticles ( $\text{Fe}_2\text{O}_3\text{-Np}$ ) using *R. mucronata* was very fast and required no toxic chemicals. Synthesized  $\text{Fe}_2\text{O}_3\text{-Np}$  was confirmed by colour change, and based on UV-visible spectroscopy analysis, where a  $\lambda$  max of 368.0 nm was observed. The  $\text{Fe}_2\text{O}_3\text{-Np}$  were stable up to 3 months and exhibited an excitation at 368.0 nm and emission at 370.5 nm. FTIR spectrum revealed the changes of functional groups during the formation iron (III) oxide nanoparticles. The average lattice size found for  $\text{Fe}_2\text{O}_3\text{-Np}$  ranged from 1.14 to 4.55 nm based on XRD analysis and mean particle size distribution in aqueous media was about 65 nm. TEM analysis revealed a smaller particle size of 5.58 – 9.02 nm that was in agreement with SAED analysis. The synthesized  $\text{Fe}_2\text{O}_3\text{-Np}$  exhibited a good photodegradation efficiency with a reduction of 83 and 95% of phenol red and crystal violet under irradiation of sunlight and florescent light respectively.

#### 5 Acknowledgments

The authors are grateful to the Director, NIO, Goa and Scientist- in- charge, CSIR-NIO (RC), Kochi for their support and advice. NVK acknowledge the financial support of Science and Engineering Board (SERB), Government of India through National Post-Doctoral fellowship [PDF/2016/000438]. This is NIO contribution number xxxx. Authors acknowledge Central Instrumentation Unit, Lady Doak College, Madurai for photoluminescence analysis and Sophisticated Test and Instrumentation Centre (STIC), CUSAT for XRD and TEM analysis; Karunya University, Coimbatore for DSL, SEM and EDAX.



## 6 References

- [1] Mandal, D., Bolander, M.E., Mukhopadhyay, D., et al.: The use of microorganisms for the formation of metal nanoparticles and their application, *Appl. Microbiol. Biotechnol.*, 2006, 69, pp- 485-492.
- [2] Jebali, A., Ramezani, F., Kazemi, B., Biosynthesis of silver nanoparticles by *Geotricum sp.*, *J. Clust. Sci.*, 2011, 22, pp- 225-232.
- [3] Iravani, S., Green synthesis of metal nanoparticles using plants, *Green Chem.*, 2011, 13, pp-2638-2650.
- [4] Dhillon, G.S., Brar, S.K., Kaur, S., et al.: Green approach for nanoparticle biosynthesis by fungi: current trends and applications, *Crit. Rev. Biotechnol.*, 2012, 32, pp- 49-73.
- [5] Kalaiarasi, R., Jayalakshmi, N., Venkatachalam, P., Phytosynthesis of nanoparticles and its applications, *Plant Cell Biotechnol. Mol. Biol.*, 2010, 11, pp- 1-16.
- [6] Lin, W., Rieter, W.J., Taylor, K.M., Modular synthesis of functional nanoscale coordination polymers, *Angewandte Chemie International Edition*, 2009, 48, pp- 650-658.
- [7] Gouda, S., Das, G., Sen, S.K., et al.: Mangroves, a potential source for green nanoparticle synthesis: a review, *IJMS*, 2015, 44, pp- 635-645.
- [8] Premanathan, M., Benitha, V.S.S., Jeyasubramanian, K., et al.: Rapid Biosynthesis of antibacterial silver nanoparticles by *Rhizophora mucronata* leaf, *Adv. Sci. Eng. Med*, 2014, 6, pp- 184-187.
- [9] Gnanadesigan, M., Anand, M., Ravikumar, S., et al.: Biosynthesis of silver nanoparticles by using mangrove plant extract and their potential mosquito larvicidal property, *Asian Pac. J. Trop. Med*, 2011, 4, pp- 799-803.
- [10] Dai, K., Chen, H., Peng, T., et al.: Photocatalytic degradation of methyl orange in aqueous suspension of mesoporous titania nanoparticles, *Chemosph.*, 2007, 69, pp- 1361-1367.
- [11] Dipti, V., Sharma, V.K., Study of synthesis and photocatalytic activities of Mo doped ZnO, *J. Chem. Pharmaceut. Res*, 2010, 2, pp- 269-273.
- [12] Leland, J.K., Bard, A.J., Photochemistry of colloidal semiconducting iron oxide polymorphs, *J. Physic. Chem.*, 1987, 91, pp- 5076-5083.
- [13] Zhao, S., Wu, H.Y., Song, L., et al.: Preparation of  $\gamma$ -Fe<sub>2</sub>O<sub>3</sub> nanopowders by direct thermal decomposition of Fe-urea complex: reaction mechanism and magnetic properties, *J. Mat. Sci.*, 2009, 44, pp- 926-930.
- [14] Bharathi, S., Nataraj, D., Mangalaraj, D., et al.: Highly mesoporous  $\alpha$ -Fe<sub>2</sub>O<sub>3</sub> nanostructures: preparation, characterization and improved photocatalytic performance towards Rhodamine B (RhB), *J. Phys. D: Appl. Phys.*, 2009, 43, pp- 015501.
- [15] Abraham, S.D., David, S.T., Bennie, R.B., et al.: Eco-friendly and green synthesis of BiVO<sub>4</sub> nanoparticle using microwave irradiation as photocatalyst for the degradation of Alizarin Red S, *J. Mol. Struct.*, 2016, 1113, pp. 174-181.
- [16] Pattanayak, M., Nayak, P.L., Ecofriendly green synthesis of iron nanoparticles from various plants and spices extract, *Int. J. Plant, Anim. Environ. Sci.*, 2013, 3, pp- 68-78.

- [17] Song, J.Y., Kim, B.S., Rapid biological synthesis of silver nanoparticles using plant leaf extracts, *Biopro. Biosys. Eng.*, 2009, 32, pp-79.
- [18] Ocaña, M., Morales, M.P., Serna, C.J., Homogeneous precipitation of uniform  $\alpha$ -Fe<sub>2</sub>O<sub>3</sub> particles from iron salts solutions in the presence of urea, *J. Coll. Interf. Sci.*, 1999, 212, pp-317-323.
- [19] Balamurugan, M., Saravanan, S., Soga, T., Synthesis of iron oxide nanoparticles by using *Eucalyptus globulus* plant extract, *e-J. Surf. Sci. Nanotechnolo.*, 2014, 12, pp- 363-367.
- [20] Masarovičová, E., Kráľová, K., Metal Nanoparticles and Plants/Nanocząstki Metaliczne I Rośliny, *Ecolog. Chem. Eng.*, 2013, 20, pp- 9-22.
- [21] Alqudami, A., Annapoorni, S.: Fluorescence from metallic silver and iron nanoparticles prepared by exploding wire technique, *Plasmonics*, 2007, 2, pp. 5-13.
- [22] Mahdavi, M., Namvar, F., Ahmad, M.B., et al.: Green biosynthesis and characterization of magnetic iron oxide (Fe<sub>3</sub>O<sub>4</sub>) nanoparticles using seaweed (*Sargassum muticum*) aqueous extract, *Molec.*, 2013, 18, pp- 5954-5964.
- [23] Nakamoto, K., Nakamoto, K., Infrared and Raman spectra of inorganic and coordination compounds, Wiley, 1977.
- [24] Sharma, V.K., Pandey, O.P., Sengupta, S.K., Synthesis and physico-chemical and biological studies on ruthenium (III) complexes with Schiff bases derived from aminocarboxylic acids, *Trans. Metal Chem.*, 1987, 12, pp- 509-515.
- [25] Gottimukkala, K.S.V., Green synthesis of iron nanoparticles using green tea leaves extract, *J. Nanomed. Biotherap. Dis.*, 2017, 7, pp- 151.
- [26] Ahmmad, B., Leonard, K., Islam, M. S., et al.: Green synthesis of mesoporous hematite ( $\alpha$ -Fe<sub>2</sub>O<sub>3</sub>) nanoparticles and their photocatalytic activity. *Advan. Powder Technolo.*, 2013, 24(1), 160-167.
- [27] Dhahir, S.A., AL-Saade, K.A., AL-Jobouri, I.S., Degradation studies of rhodamine B in the presence of UV/H<sub>2</sub>O<sub>2</sub>/Fe<sub>2</sub>, *Int. J. Tech. Res. Appl.*, 2014.
- [28] Alshehri, A., Malik, M.A., Khan, Z., et al.: Biofabrication of Fe nanoparticles in aqueous extract of *Hibiscus sabdariffa* with enhanced photocatalytic activities, *RSC Advances*, 2017, 7, pp. 25149-25159.
- [29] Chowdhury, P.R., Bhattacharyya, K.G., Synthesis and characterization of Co/Ti layered double hydroxide and its application as a photocatalyst for degradation of aqueous Congo Red, *RSC Adv.*, 2015, 5, pp- 92189-92206.